




Article

Mechanical Alloying and Hot Pressing of Ti-Zr-Si-B Powder Mixtures

Isadora Rossi Bertoli ¹, Lucas Moreira Ferreira ², Bruno Xavier de Freitas ² , Carlos Angelo Nunes ² , Alfeu Saraiva Ramos ¹, Marcello Filgueira ³, Claudinei dos Santos ⁴  and Erika Coaglia Trindade Ramos ^{1,*}

¹ Instituto de Ciência e Tecnologia, Universidade Federal de Alfenas, Rodovia José Aurélio Vilela, 11999, Poços de Caldas, MG 37715-400, Brazil; isadorarbertoli@gmail.com (I.R.B.); alfeu.ramos@unifal-mg.edu.br (A.S.R.)

² Departamento de Engenharia de Materiais, Escola de Engenharia de Lorena, Universidade de São Paulo, Polo Urbo Industrial, Gleba AI-6, Lorena, SP 12602-810, Brazil; lucasmofe@gmail.com (L.M.F.); bxfreitas@usp.br (B.X.d.F.); cnunes@eel.usp.br (C.A.N.)

³ Centro de Ciências e Tecnologia, Universidade Estadual do Norte Fluminense Darcy Ribeiro, Avenida Alberto Lamengo, 200, Parque Califórnia, Campos de Goytacazes, RJ 28013-602, Brazil; marcello@uenf.br

⁴ Faculdade de Tecnologia de Resende, Universidade do Estado do Rio de Janeiro, Rodovia Presidente Dutra km 298, Polo Industrial de Resende, Resende, RJ 27537-000, Brazil; claudineisvr@gmail.com

* Correspondence: erika.ramos@unifal-mg.edu.br; Tel.: +55-35-3697-4735

Received: 12 December 2017; Accepted: 17 January 2018; Published: 23 January 2018

Abstract: This work discusses microstructure evolution during ball milling and hot pressing of Ti- x Zr-10Si-5B ($x = 2$ and 5 at. %) and Ti- x Zr-20Si-10B ($x = 5, 7, 10, 15$ and 20 at. %) powder mixtures. Mechanical alloying was carried out in a ball mill using stainless steel balls and vials, 300 rpm and a ball-to-powder ratio of 10:1. Powders milled for 600 min were then hot-pressed (25 MPa) under vacuum at 1100 °C for 60 min. As-milled and hot-pressed samples were evaluated by X-ray diffraction (XRD), scanning electron microscopy (SEM), differential scanning calorimetry (DSC), and energy dispersive spectrometry (EDS). Peaks of Si and Zr disappeared in powders milled for 60 and 180 min, respectively, while the lattice parameters and cell volume of α -Ti were varied during ball milling up to 300 min indicating that supersaturated solid solutions were achieved. Ti₆Si₂B dissolving up to 10 at. % Zr was found in microstructure of hot-pressed Ti- x Zr-10Si-5B ($x = 2$ and 5 at. %) and Ti- x Zr-20Si-10B ($x = 2, 5, 7$ and 10 at. %) alloys. The amount of TiB and Ti₅Si₃ was preferentially increased whereas the Ti₃Si formed in microstructure of the hot-pressed Ti-15Zr-20Si-5B and Ti-20Zr-20Si-10B alloys.

Keywords: mechanical alloying; hot pressing; phase transformation; titanium alloy; Ti₆Si₂B; biomaterial; high temperature

1. Introduction

Titanium alloys are widely used to produce different orthopedic devices and high-temperature structural components such as artificial hip joints and gas turbine components, respectively [1–5]. However, Co-Cr and Co-Cr-Mo alloys are also utilized as articular component in hip joints owing to their superior wear resistance than the conventional Ti alloys [6–8]. In this way, the improved wear resistance of new Ti alloys containing the Nb, Ta and/or Zr addition is limited because their microstructures are based on substitutional solid solutions [9]. In addition, new Ti alloys based on intermetallic TiAl compounds have been developed to fabricate turbochargers and gas turbines [10].

Previous works have reported on the present good biocompatibility and wear resistance of the Ti-Si alloys which are formed by the Ti and Ti₅Si₃ phases [11,12] as well as the detrimental Ti₅Si₃ formation in these alloys mainly due to its high crystallographic anisotropy [13]. Two-phase Ti+Ti₆Si₂B

alloys are successfully produced from elemental starting materials by arc melting and mechanical alloying, which are attractive for structural application due to their better oxidation resistance and low crystallographic anisotropy than the Ti-Si alloys and the Ti_5Si_3 compound, respectively [14–17]. After heat treatment or sintering, the metallic or ceramic matrix composites based on the Ti_{ss} (ss-solid solution) and $\text{Ti}_6\text{Si}_2\text{B}$ phases are formed in the Ti-10Si-5B and Ti-20Si-10B alloys, respectively [17]. However, small amounts of TiB and Ti_5Si_3 can be still found in heat treated or sintered Ti-Si-B alloys owing the narrow composition range in the two-phase Ti+ $\text{Ti}_6\text{Si}_2\text{B}$ region [17]. In this sense, the high-energy ball milling has produced homogeneous materials with nanosized structures, reducing the diffusion paths needed to reach the equilibrium microstructure [18,19].

Previous work has indicated that the Ti- x Mo-22Si-11B ($x = 2, 5, 7$ and 10 at. %) alloys produced by mechanical alloying and subsequent sintering have dissolved small Mo amounts close to 2 at. % into the $\text{Ti}_6\text{Si}_2\text{B}$ lattice. Larger amounts of Ti_5Si_3 and TiB formed in microstructure of these quaternary alloys with increase of Mo addition in the alloy composition [20].

Studies involving the Ti-Si alloys constituted by the Ti_{ss} (matrix) and Ti_5Si_3 phases have revealed that the added zirconium dissolved preferentially into the Ti_5Si_3 lattice, and contributed to improve their oxidation resistance [21–23]. Significant amounts of zirconium close to 6 at. % were dissolved into the $\text{Ti}_6\text{Si}_2\text{B}$ lattice of Ti-Zr-Si-B alloys produced by arc melting and subsequent heat treatment [24].

In this regard, this work reports on microstructure evolution during ball milling and subsequent hot pressing of Ti- x Zr-10Si-5B ($x = 2$ and 5 at. %) and Ti- x Zr-20Si-10B ($x = 2, 5, 10, 15$ and 20 at. %) materials potentially attractive for the development of artificial hip joints and high-temperature structural components.

2. Materials and Methods

2.1. Specimen Preparation

Mechanical alloying and subsequent hot pressing were used to produce the Ti-2Zr-10Si-5B, Ti-5Zr-10Si-5B, Ti-5Zr-20Si-10B, Ti-10Zr-20Si-10B, Ti-15Zr-20Si-10B, and Ti-20Zr-20Si-10B (at. %) alloys in the present investigation using Ti (99.9 wt %, <150 mesh, spherical), Si (99.995 wt %, <100 mesh, irregular), B (99.5 wt %, <120 mesh, angular), and Zr (chips with min 95.5 wt % and containing up to 4.5 wt % Hf) as starting materials (Alfa Aesar, Ward Hill, MA, USA).

The solid-state processing of Ti-Zr-Si-B powder mixtures was carried out in a planetary Fritsch P-5 ball mill (Fritsch GmbH, Idar-Oberstein, Germany) using stainless steel balls (19 mm diameter) and vials (225 mL), 300 rpm and a ball-to-powder weight ratio of 10:1. To evaluate on phase transformation in the Ti-Zr-Si-B powder mixtures, samples were taken from the vials after different times: 20, 60, 300, 420 and 600 min. To avoid the atmosphere contamination and exothermic reactions, the powder mixtures were handled into the Ar-flushed glove box (MBRAUN Co., Garching, Germany).

Hot pressing of Ti-Zr-Si-B powders previously milled for 600 min was performed in a Thermal Technology Inc. model Astro 1000 equipment (Thermal Technology LLC, Santa Rosa, CA, USA) using high vacuum (10^{-6} Torr), pressure levels of 25 MPa, and a BN-coated graphite crucible. After reaching 1100 °C for 60 min under heating rate of 10 °C/min, samples were then furnace cooled to room temperature.

2.2. Microstructure Evaluation

Phase transformations during ball milling and hot pressing of the Ti-Zr-Si-B powder mixtures were evaluated by means of X-ray diffraction (XRD) (PANalytical, Almelo, The Netherlands), scanning electron microscopy (SEM) (Carl Zeiss AG GmbH, Gena, Germany), differential scanning calorimetry (DSC) (NETZSCH Group, Selb, Bavaria, Germany), and energy dispersive spectrometry (EDS) (Carl Zeiss SMT Ltd., Oberkochen, Germany) techniques.

Electron images were acquired in a ZEISS model EVO MA-10 SEM using the backscattered electron (BSE) detector (Carl Zeiss SMT Ltd., Oberkochen, Germany). The Ti, Zr and Si contents of the

phases formed in microstructure of hot-pressed Ti-Zr-Si-B alloys were measured by EDS analysis using inner patterns.

XRD experiments at room temperature were performed in a Philips PW 3719 equipment using Ni-filtered Cu-K α radiation, angular interval (2θ) from 10 to 90°, angular step of 0.05°, and counting time of 3 s. The phases formed in Ti-Zr-Si-B samples were initially indexed from the JCPDS database [25] and the Powdercell computer program [26]. From these XRD patterns, the values of α -Ti lattice parameters and cell volume as well as the α -Ti (101) plane distance and amount of present phases in Ti-Zr-Si-B powders milled up to 300 min were determined by Rietveld refining using the Fullprof version 2.7.9 computer program [27], whereas the sizes of crystallite were calculated using the Scherrer equation ($D = 0.9\lambda/\beta\cos\theta$). The structure refining was difficult in XRD patterns of Ti-Zr-Si-B powders milled for longer times owing the presence of severely deformed structures.

DSC experiments of Ti-Zr-Si-B powders milled for 600 min were performed in a Netzsch model STA Jupiter F3 instrument (NETZSCH Group, Selb, Bavaria, Germany) under dynamic high-purity Ar atmosphere and a heating rate of 10 °C/min using alumina crucible.

3. Results and Discussion

3.1. Mechanical Alloying

The Ti-2Zr-10Si-5B and Ti-5Zr-10Si-5B powder mixtures presented similar milling behavior during ball milling. Figure 1a shows the XRD pattern of Ti-5Zr-10Si-5B powders milled at different times. Peaks of Ti, Zr and Si were noted in XRD pattern of these powders milled for 20 min. Following, the Si peaks disappeared in these powders milled for 60 min suggesting that the Si atoms were dissolved into the Ti cell to form supersaturated Ti solid solutions. Peaks of Zr disappeared after milling for 180 min. No significant change has occurred in Ti- x Zr-10Si-5B ($x = 2$ and 5 at. %) powders milled for 600 min, and the Ti peaks can be achieved only.

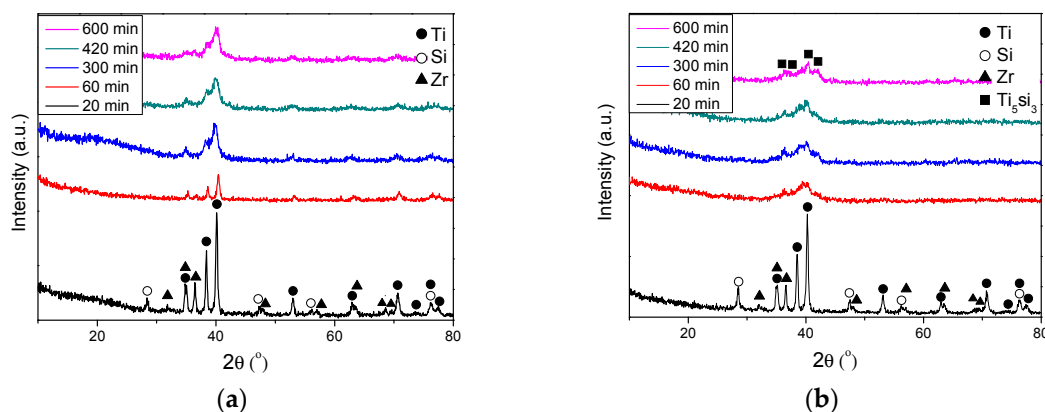


Figure 1. XRD patterns of: (a) Ti-5Zr-10Si-5B; and (b) Ti-5Zr-20Si-10B powder mixtures at different milling times.

Similar behavior was observed during ball milling of the Ti-5Zr-20Si-10B, Ti-10Zr-20Si-10B, Ti-15Zr-20Si-10B and Ti-20Zr-20Si-10B powder mixtures. XRD patterns of Ti-10Zr-20Si-10B powders milled for different times are presented in Figure 1b. Peaks of Ti₅Si₃ were indexed in XRD patterns of these powder mixtures milled for 60 min, which were more pronounced with the increase of milling time. In the sequence, no significant change occurred in Ti- x Zr-20Si-10B ($x = 5, 10, 15$ and 20 at. %) samples milled up to 600 min.

The amount of present phases in Ti-Zr-Si-B powders milled up to 300 min is presented in Table 1, which are determined by Rietveld refining. Results have indicated that the Zr and Si amounts were promptly reduced after milling for 20 and 60 min of Ti-2Zr-10Si-5B and Ti-5Zr-10Si-5B powders, respectively, suggesting that the Zr and Si atoms were dissolved into the α -Ti cell. Similar behavior on

the reduced Si amount was found during ball milling for 300 min of Ti- x Zr-20Si-10B ($x = 5, 10, 15$ and 20 at. %) powders. Contrarily, the amounts of Ti and Zr increased in these powder mixtures milled up to 60 min, suggesting that the supersaturated Ti and Zr solid solutions were achieved. Only α -Ti was measured from the XRD patterns of Ti- x Zr-20Si-10B ($x = 5, 10$ and 15 at. %) powders milled for 300 min, while that the amounts of Ti, Zr and Si were not determined in Ti-20Zr-20Si-10B powders milled for 300 min due to the severely deformed structures and Ti_5Si_3 formation.

Table 1. Amount of present phases in Ti-Zr-Si-B powders milled up to 300 min.

Milling Time	Ti	Zr	Si
Ti-2Zr-10Si-5B			
20	95.11	1.59	3.3
60	100	0	0
300	100	0	0
Ti-5Zr-10Si-5B			
20	80.41	6.61	12.99
60	95.35	4.65	0
300	100	0	0
Ti-5Zr-20Si-10B			
20	55.06	8.68	36.26
60	70.42	8.68	20.89
300	100	0	0
Ti-10Zr-20Si-10B			
20	61.5	7.2	31.3
60	82.15	14.33	3.53
300	100	0	0
Ti-15Zr-20Si-10B			
20	51.66	11.62	36.72
60	76.29	18.39	5.32
300	100	0	0
Ti-20Zr-20Si-10B			
20	50.31	18.62	31.07
60	58.67	29.21	12.12
300	ND	ND	ND

ND: Not Determined.

Figure 2a shows the effect of composition on X-ray scattering of major α -Ti peaks in Ti-Zr-Si-B samples milled for 60 min. No significant change was noted in the Ti- x Zr-10Si-5B ($x = 2$ and 5 at. %). In contrast, it can be observed that the intensity of the (101) and (002) peaks was reduced with the zirconium increased in the Ti- x Zr-20Si-10B ($x = 5, 10, 15$ and 20 at. %) powder mixture due to the higher distortion in α -Ti lattice.

Effect of composition and milling time on interplanar distance “ d ” of α -Ti (101) crystal plane mechanically alloyed in the Ti-Zr-Si-B powder mixtures are illustrated in Figure 2b. Results have indicated that the “ d ” values varied owing to the formation of supersaturated α -Ti solid solutions. Despite the similar characteristics between the major α -Ti peaks in XRD patterns of Ti-2Zr-10Si-5B and Ti-5Zr-10Si-5B powders milled for 60 min (see Figure 2a), their d values were varied oppositely in powders milled for 20 and 60 min, and they were similar in these powders milled for 300 min. Excepting to the Ti-20Zr-20Si-10B powders milled for 300 min, the “ d ” values were continuously reduced during milling for 300 min of the Ti- x Zr-20Si-10B ($x = 5, 10, 15$ and 20 at. %) powder mixtures. Results have indicated that the lower d values occurred owing the dissolution of larger amounts of smaller Si and B atoms than the lesser amounts of larger Zr atoms into the α -Ti cell during their processing by ball milling. In addition, it was also noted that the α -Ti (101) plane distance was increased for these Zr-rich powder mixtures milled for 300 min.

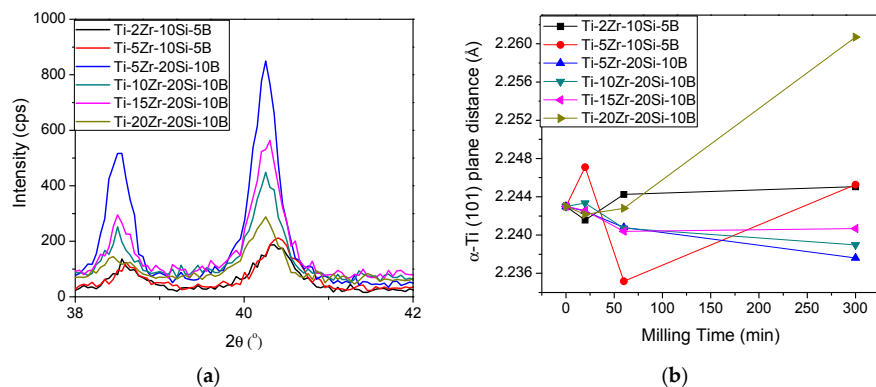


Figure 2. (a) X-ray scattering on the major α -Ti peaks in Ti-Zr-Si-B powder mixtures milled for 60 min; and (b) interplanar distance “ d ” of α -Ti (101) crystal plane as a function of composition and milling time in the Ti-Zr-Si-B powder mixtures.

The lattice parameters and cell volume of α -Ti in the Ti-Zr-Si-B powders milled up to 300 min are displayed in Figure 3. Coherent with the d values found for these powder mixtures, a similar behavior was noted for these ones. After milling for 20 min, the Ti-5Zr-10Si-5B powders exhibited larger lattice parameters and cell volume values than the Ti-2Zr-10Si-5B powders, whereas both the powder mixtures indicated the near a lattice parameter values. Contrarily, the Ti-5Zr-10Si-10B powders presented the higher c lattice parameter and cell volume values in α -Ti than the Ti-2Zr-10Si-5B powders milled for 300 min mainly due to the higher amounts of Zr dissolved in its cell. Excepting to the Ti-20Zr-20Si-10B powders milled for 300 min, the a lattice parameter and cell volume of α -Ti were slightly reduced in the Ti- x Zr-20Si-10B ($x = 5, 10, 15$ and 20 at. %) powders milled up to 300 min. Contrary to this previously mentioned behavior, the c lattice parameters of α -Ti were slightly increased in the Ti- x Zr-20Si-10B ($x = 5, 15$ and 20 at. %) powders milled for 300 min.

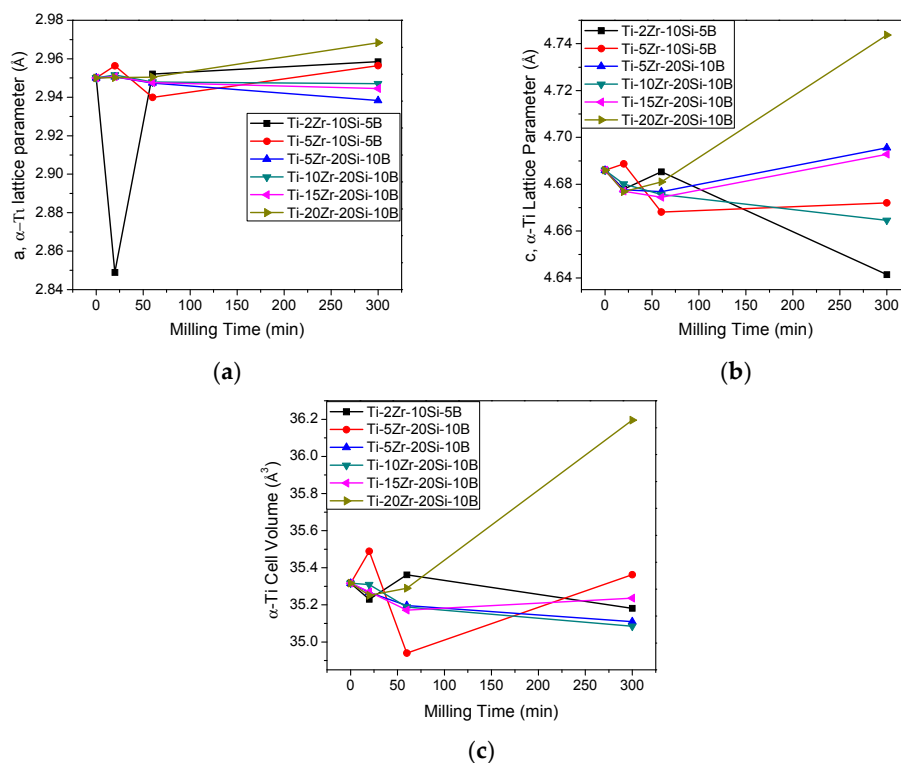


Figure 3. Effect of composition and milling time on the: (a,b) lattice parameters; and (c) cell volume of α -Ti in the Ti-Zr-Si-B powder mixtures.

Figure 4 shows the effect of composition and milling time on the Zr lattice parameters and cell volume. As previously discussed, a partial Zr amount was dissolved into the α -Ti cell during ball milling of Ti-Zr-Si-B powders up to 300 min. Nonetheless, the Si atoms were also dissolved into the Zr lattice during 20 and 60 min. Consequently, the cell volume was also decreased at these times.

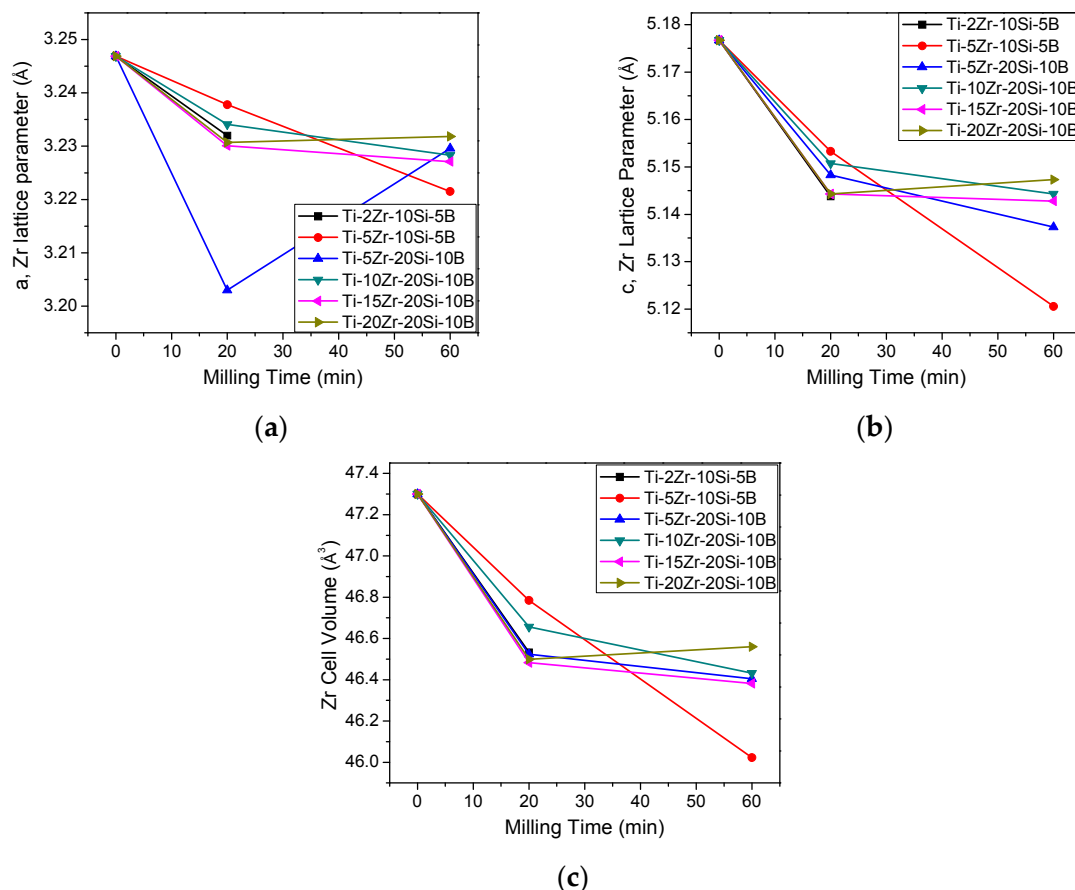


Figure 4. Effect of composition and milling time on the: (a,b) lattice parameters; and (c) cell volume of Zr in the Ti-Zr-Si-B powder mixtures.

The crystallite sizes of Ti of mechanically alloyed Ti- x Zr-Si-B ($x = 2, 5, 10, 15$ and 20 at. %) powders are presented in Figure 5. In the Ti- x Zr-10Si-5B powders ($x = 2$ and 5 at. %), the sizes of crystallite were continuously reduced with the increase milling time, except for the Ti-2Zr-10Si-5B powders milled for 600 min. Sizes of crystallite were initially reduced in the Ti- x Zr-20Si-10B ($x = 5, 10, 15$, and 20 at. %) powders milled up to 300 min, which were subsequently increased during milling up to 600 min. As previously mentioned, the heat released from exothermic Ti_5Si_3 reaction has contributed for reducing the number of defects provided during ball milling and, consequently, the amount of number of sites available to form the supersaturated solid solutions. Other study has also reported on formation of metastable structures in mechanical alloyed Ti-Si powders [28]. Moreover, the results indicated that the zirconium addition has contributed to reduce the Ti crystallite sizes, denoting that its addition provided higher distortion into the Ti lattice and favored the occurrence more effective between the cold welding and fracture mechanisms during ball milling of the Ti- x Zr-20Si-10B powder mixtures. Previous work has also reported on the preparation of nanocrystalline Ti-Si powders by mechanical alloy [29].

SEM images of mechanically alloyed Ti-Zr-Si-B powders milled at different times are presented in Figure 6. Initially, the particles of Ti, Zr/Si and B powders presented morphologies spherical, irregular and angular, respectively. It can be noted that the size of particles was increased continuously in

Ti-Zr-Si-B powders milled up to 180 min owing to the intense cold-welded mechanisms between the ductile particles. As expected, this mechanism was more accentuated for the Ti- x Zr-10Si-5B ($x = 2$ and 5 at. %) powder mixtures containing larger amounts of ductile components. Following, the sizes of particles of Ti-Zr-Si-B powders were reduced after milling for 300 min, indicating that the fracture mechanisms were more effective than those previous cold-welding mechanism. In the Ti-2Zr-10Si-5B and Ti-5Zr-10Si-5B powder mixtures, the hardening mechanisms by cold work and solid solution have contributed to reduce the particle sizes while the in situ formation of brittle Ti_5Si_3 phase contributed for reduction on the particles sizes of the Ti- x Zr-20Si-10B ($x = 10, 15$ and 20 at. %) powders. After milling for 600 min, the Ti-Zr-Si-B powder mixtures presented more uniform particle size distribution beyond the presence of aggregated fine particles.

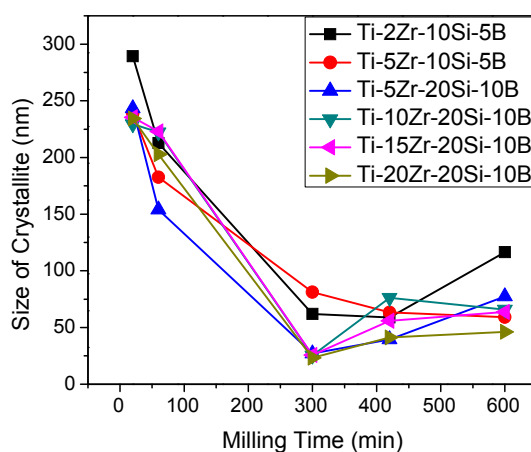


Figure 5. Effect of milling time on the Ti crystallite sizes in Ti-Zr-Si-B powder mixtures.

The DSC curves obtained during heating of mechanically alloyed Ti- x Zr-20Si-10B ($x = 5, 10, 15$ and 20 at. %) powders milled for 600 min are illustrated in Figure 7. It can be noted the occurrence of two exothermic peaks located near the 500 °C and 950 °C. According to the X-ray diffraction analysis, these exothermic peaks are related to the formation of intermetallic phases such as $\text{Ti}_6\text{Si}_2\text{B}$, Ti_5Si_3 , and TiB. Table 2 presents the peak temperature as well as the heat flow and enthalpy values relative to the major exothermic peak identified in DSC curves during heating of Ti- x Zr-20Si-10B ($x = 5, 10, 15$ and 20 at. %) powders milled for 600 min. Results have indicated that the DSC peak temperature varied between 502.9 and 521.8 °C from the powder mixtures with 5 and 20 at. % Zr, respectively. Excepting to the powder mixture containing 20 at. % Zr, it was also noted that the enthalpy values (and released heat flow) increased from 498.2 kJ/kg (1.383 mW/mg) to 1008.3 kJ/kg (2.792 mW/mg) in Ti-5Zr-20Si-10B and Ti-15Zr-20Si-10B powders, respectively, which could be related to the previously metastable structures formed during mechanical alloying.

Table 2. DSC peak temperature, released heat flow and enthalpy values relative to the major exothermic event occurred during heating of mechanically alloyed Ti- x Zr-20Si-11B ($x = 5, 10, 15$ and 20 at. %) powders milled for 600 min.

Alloy	Peak Temperature (°C)	Released Heat Flow (mW/mg)	Enthalpy (kJ/kg)
Ti-5Zr-20Si-10B	506.0	1.383	498.2
Ti-7Zr-20Si-10B	502.9	1.898	708.9
Ti-10Zr-20Si-10B	505.6	2.504	851.2
Ti-15Zr-20Si-10B	521.8	2.792	1008.3
Ti-20Zr-20Si-10B	518.6	2.076	679.6

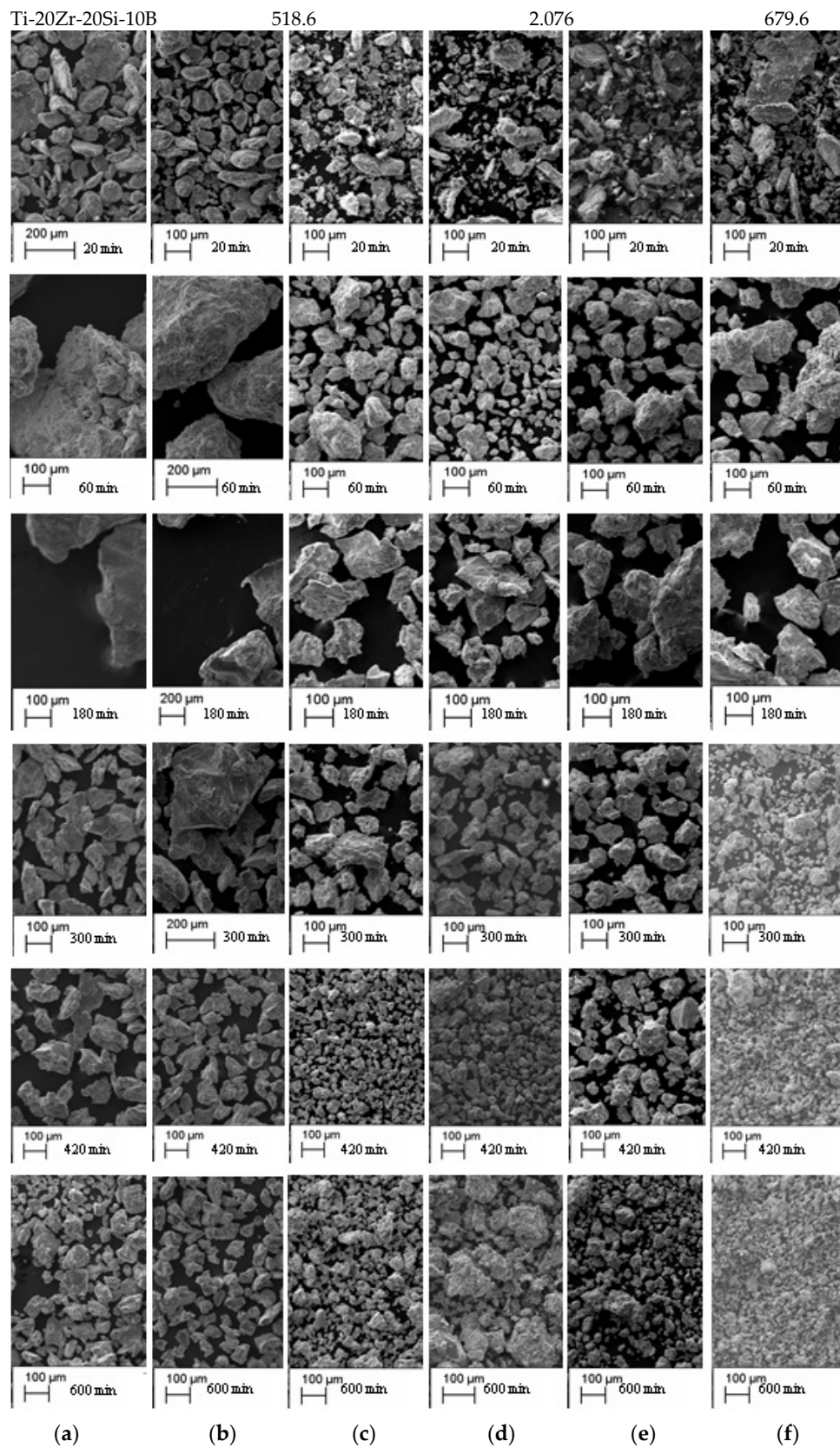


Figure 6. SEM images of: (a) Ti-2Zr-10Si-5B; (b) Ti-5Zr-10Si-5B; (c) Ti-5Zr-20Si-10B; (d) Ti-10Zr-20Si-10B; (e) Ti-15Zr-20Si-10B; and (f) Ti-20Zr-20Si-10B powder mixtures after different milling times.

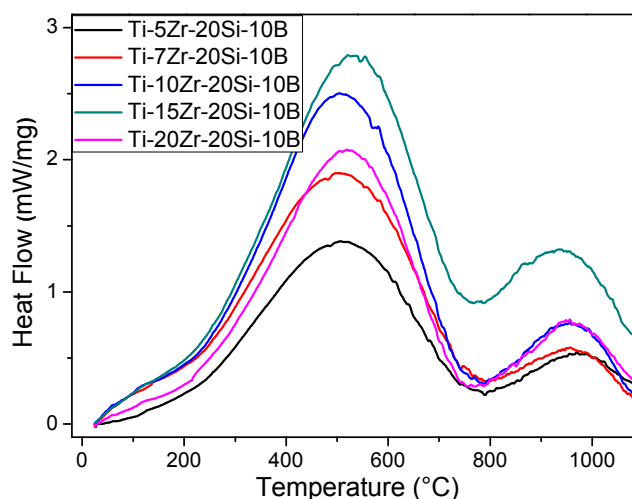


Figure 7. DSC curves of mechanically alloyed Ti-*x*Zr-20Si-10B (*x* = 5, 10, 15 and 20 at. %) powders previously milled for 600 min showing the existence of two exothermic peaks near the 500 °C and 950 °C.

3.2. Hot Pressing

Figure 8 shows the XRD patterns of Ti-Zr-Si-B alloys produced by mechanical alloying and subsequent hot pressing. Only the peaks of Ti and $\text{Ti}_6\text{Si}_2\text{B}$ were indexed in XRD spectra of the mechanically alloyed and hot pressed Ti-*x*Zr-10Si-5B (*x* = 2 and 5 at. %) alloys (Figure 8a). In addition, the peaks of $\text{Ti}_6\text{Si}_2\text{B}$ were moved toward the lower diffraction angles due to the Zr dissolution into its lattice in order to form solid solution. Peaks of Ti_5Si_3 beyond the Ti and $\text{Ti}_6\text{Si}_2\text{B}$ phases were identified in XRD patterns of the mechanically alloyed and hot-pressed Ti-5Zr-20Si-10B (Figure 8b) and Ti-10Zr-20Si-10B (Figure 8c) alloys. No evidence of $\text{Ti}_6\text{Si}_2\text{B}$ was identified in XRD patterns of the mechanically alloyed and hot-pressed Ti-15Zr-20Si-10B (Figure 8d) and Ti-20Zr-20Si-10B (Figure 8e) alloys, while only the peaks of Ti, TiB, Ti_3Si and Ti_5Si_3 could be indexed, indicating that the production of $\text{Ti}_6\text{Si}_2\text{B}$ -based Ti-Zr-Si-B alloys are limited for zirconium additions of up to 10 at. %.

The lattice parameters and cell volume of Ti, $\text{Ti}_6\text{Si}_2\text{B}$, TiB and/or Ti_5Si_3 formed in microstructure of the mechanically alloyed and hot-pressed Ti-5Zr-10Si-5B, Ti-5Zr-20Si-10B, Ti-15Zr-20Si-10B and Ti-20Zr-20Si-10B alloys calculated by Rietveld refining are presented in Table 3. α -Ti and Ti_5Si_3 present *a/c* lattice parameters (and cell volume) of 2.95/4.686 Å (35.317 Å³) and 7.444/5.143 Å (246.81 Å³), respectively. Despite the lesser *a* lattice parameters of α -Ti (in Ti-20Zr-20Si-10B alloy) and Ti_5Si_3 (in Ti-15Zr-20Si-10B alloy), the cell volume of α -Ti and Ti_5Si_3 were increased in these alloys due to the Zr dissolution. Similar dissolution behavior was noted in TiB cell. No Rietveld refining of $\text{Ti}_6\text{Si}_2\text{B}$ and Ti_3Si was possible due to its extremely distorted peaks in XRD pattern.

SEM images of the Ti-5Zr-10Si-5B, Ti-5Zr-20Si-10B, Ti-10Zr-20Si-10B and Ti-20Zr-20Si-10B alloys produced by mechanical alloying and subsequent hot pressing are presented in Figure 9. Hot pressing produced dense (>98% from theoretical density) and homogeneous samples containing small amounts of pores. According to the XRD results, the microstructures of the mechanically alloyed and hot-pressed Ti-5Zr-10Si-5B and Ti-5Zr-20Si-10B alloys indicated the major presence of Ti and $\text{Ti}_6\text{Si}_2\text{B}$ beyond the small amounts of disperse TiB precipitates. Larger amounts of TiB and Ti_5Si_3 were observed in microstructures of the mechanically alloyed and hot-pressed Ti-10Zr-20Si-10B alloy. In contrast, the microstructures of the mechanically alloyed and hot-pressed Ti-15Zr-20Si-10B and Ti-20Zr-20Si-10B alloys indicated the presence of the Ti, TiB and Ti_5Si_3 phases beyond other phase containing close to 20 at. % Zr and 20 at. % Si, suggesting to be the $(\text{Ti,Zr})_3\text{Si}$ phase. The Ti, $\text{Ti}_6\text{Si}_2\text{B}$ and Ti_5Si_3 phases formed in microstructure of the mechanically alloyed and hot-pressed Ti-Zr-Si-B alloys dissolved Zr contents up to 3, 10, and 17 at. %, respectively. Previous study has reported that the TiB-reinforced Ti

composites present attractive properties for automotive and aerospace applications due to their specific strength as well as superior oxidation, creep, and corrosion resistance compared to conventional Ti alloys formed by substitutional solid solutions [30]. Moreover, the use of alloying addition (in particular, molybdenum) can increase the yield strength and plasticity of Ti_5Si_3 -reinforced Ti composites [31].

Table 3. Values of lattice parameters and cell volume of Ti, $\text{Ti}_6\text{Si}_2\text{B}$, TiB and/or Ti_5Si_3 formed in microstructure of the mechanically alloyed and hot-pressed Ti-5Zr-10Si-5B, Ti-5Zr-20Si-10B and Ti-15Zr-20Si-10B alloys.

Phase	a , Lattice Parameter (Å)	c , Lattice Parameter (Å)	Cell Volume (Å ³)
Ti-5Zr-10Si-5B			
Ti	2.95771	4.71236	35.70094
$\text{Ti}_6\text{Si}_2\text{B}$	5.78801	3.75404	108.915
TiB	4.24411	-	76.44668
Ti-5Zr-20Si-10B			
Ti	2.98027	4.7986	36.90651
Ti_5Si_3	7.5088	5.18957	252.8635
Ti-15Zr-20Si-10B			
Ti	3.044011	4.54363	36.46233
Ti_5Si_3	7.34896	5.2634	246.178
Ti-20Zr-20Si-10B			
Ti	2.90648	4.59135	33.58977
Ti_5Si_3	7.39413	5.33051	252.3908

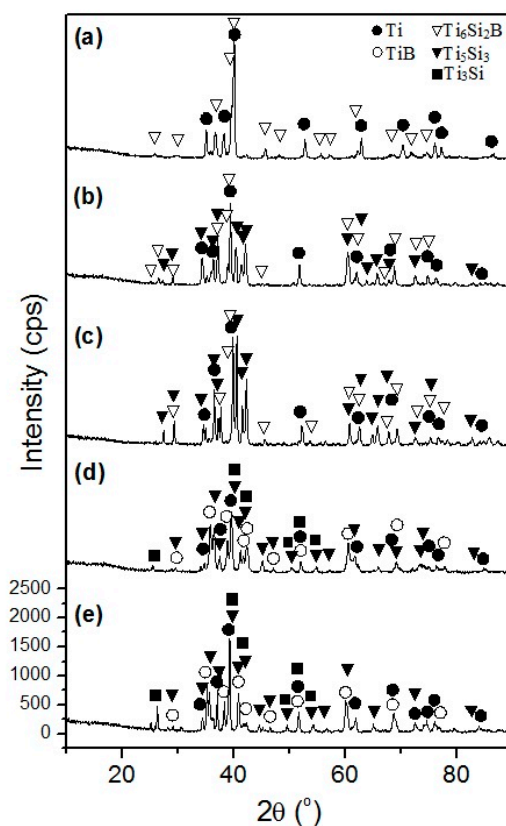


Figure 8. XRD patterns of the mechanically alloyed and hot-pressed: (a) Ti-2Zr-10Si-5B; (b) Ti-5Zr-20Si-10B; (c) Ti-10Zr-20Si-10B; (d) Ti-15Zr-20Si-10B; and (e) Ti-20Zr-20Si-10B alloys.

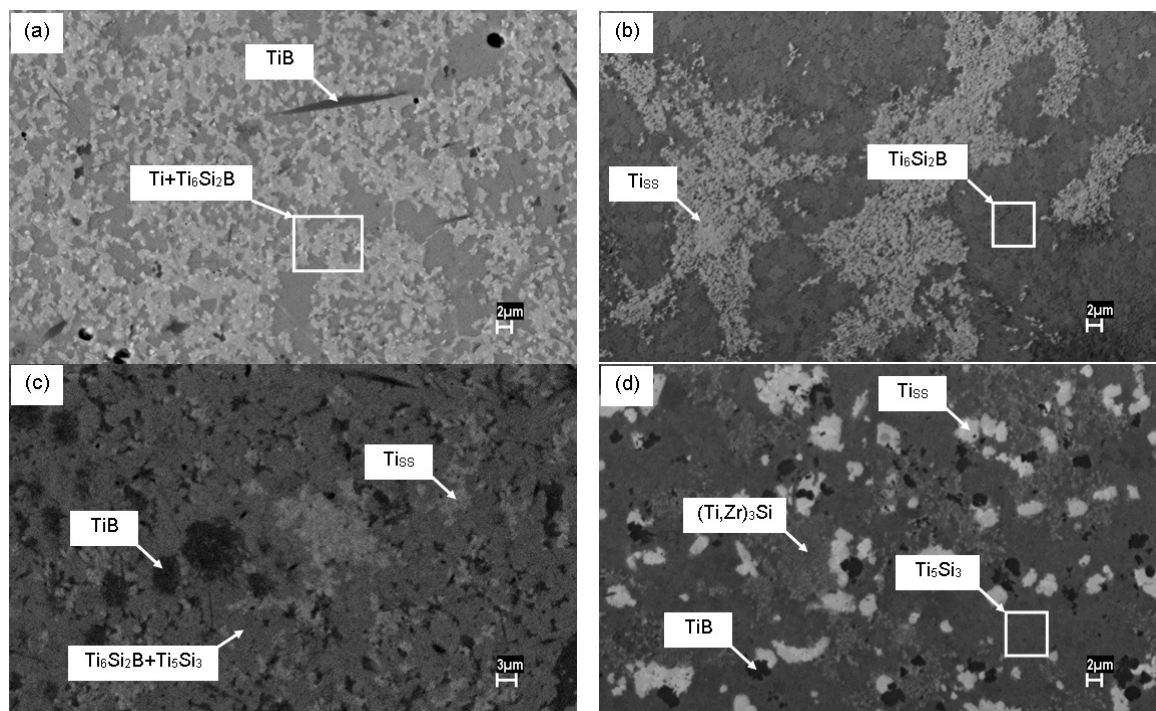


Figure 9. SEM images of the mechanically alloyed and hot-pressed: (a) Ti-5Zr-10Si-5B; (b) Ti-5Zr-20Si-10B; (c) Ti-10Zr-20Si-10B; and (d) Ti-20Zr-20Si-10B (at. %) alloys.

4. Conclusions

Mechanical alloying produced supersaturated Ti solid solutions from elemental Ti-Zr-Si-B powder mixtures. Consequently, the lattice parameters and cell volume of α -Ti cell were increased for Zr-rich powders milled for 300 min while that their crystallite sizes have been reduced.

Sizes of particles of Ti-Zr-Si-B powder mixtures increased during milling for 180 min due to excessive agglomeration of ductile particles, which were reduced at longer milling times mainly in the Zr-rich Ti-Zr-Si-B powders due to the brittle Ti_5Si_3 formation.

Mechanical alloying and hot pressing produced dense and homogeneous Ti-Zr-Si-B alloys. The Ti, $\text{Ti}_6\text{Si}_2\text{B}$, Ti_5Si_3 , and Ti_3Si phases found in microstructures of the hot-pressed Ti-Zr-Si-B alloys have dissolved up to 3, 10, 17, and 20 at. % Zr, respectively.

Two phase $\text{Ti}+\text{Ti}_6\text{Si}_2\text{B}$ alloys were successfully produced by mechanical alloying and hot pressing from the $\text{Ti}-x\text{Zr}-10\text{Si}-5\text{B}$ ($x = 2$ and 5 at. %) powder mixtures. No evidence of $\text{Ti}_6\text{Si}_2\text{B}$ was found in microstructure of the mechanically alloyed and hot pressed $\text{Ti}-x\text{Zr}-20\text{Si}-10\text{B}$ ($x = 15$ and 20 at. %) alloys.

Acknowledgments: Authors thank FAPEMIG (APQ-01119-11) and CNPq-Brazil (304890/2010-3) for financial support.

Author Contributions: Isadora Rossi Bertoli processed the Ti-Zr-Si-B powder mixtures by ball milling and the DSC analysis; Lucas Moreira Ferreira performed the XRD experiments of mechanically alloyed and hot-pressed Ti-Zr-Si-B samples; Bruno Xavier de Freitas conducted the Rietveld refining of XRD data from Ti-Zr-Si-B samples; Carlos Angelo Nunes obtained SEM images and EDS measurements of mechanically alloyed and hot-pressed Ti-Zr-Si-B samples; Alfeu Saraiva Ramos contributed starting powders and milling experiments as well as analyzed the XRD, SEM and EDS data from the mechanically alloyed and hot pressed Ti-Zr-Si-B samples; Marcello Filgueira performed the metallography and DSC experiments of mechanically alloyed and hot-pressed Ti-Zr-Si-B samples; Claudinei dos Santos designed and participated of hot-pressing experiments from the mechanically alloyed Ti-Zr-Si-B powders besides their analysis; Erika Coaglia Trindade Ramos conceived, participated and coordinate the present work in all stages as well as wrote the paper.

Conflicts of Interest: The authors declare no conflict of interest.

References

1. Prasad, K.; Bazaka, O.; Chua, M.; Rochford, M.; Fedrick, L.; Spoor, J.; Symes, R.; Tieppo, M.; Collins, C.; Cao, A.; et al. Metallic Biomaterials: Current Challenges and Opportunities. *Materials* **2017**, *10*, 884. [[CrossRef](#)] [[PubMed](#)]
2. Cremasco, A.; Messias, A.D.; Esposito, A.R.; de Rezende Duek, E.A.; Caram, R. Effects of alloying elements on the cytotoxic response of titanium alloys. *Mater. Sci. Eng. C* **2011**, *31*, 833–839. [[CrossRef](#)]
3. Chen, Q.; Thouas, G.A. Metallic implant biomaterials. *Mater. Sci. Eng. R* **2015**, *87*, 1–57. [[CrossRef](#)]
4. Whittaker, M.T.; Harrison, W.; Hurley, P.J.; Williams, S. Modelling the behaviour of titanium alloys at high temperature for gas turbine applications. *Mater. Sci. Eng. A* **2010**, *527*, 4365–4372. [[CrossRef](#)]
5. Dai, J.; Zhu, J.; Chen, C.; Weng, F. High temperature oxidation behavior and research status of modifications on improving high temperature oxidation resistance of titanium alloys and titanium aluminides: A review. *J. Alloys Compd.* **2016**, *685*, 784–798. [[CrossRef](#)]
6. Yamanaka, K.; Mori, M.; Chib, A. Assessment of precipitation behavior in dental castings of a Co–Cr–Mo alloy. *J. Mech. Behav. Biomed. Mater.* **2015**, *50*, 268–276. [[CrossRef](#)] [[PubMed](#)]
7. E, S.F.; Shi, L.; Guo, Z.G.; Liu, W.M. The recent progress of tribological biomaterials. *Biosurf. Biotribol.* **2015**, *1*, 81–97. [[CrossRef](#)]
8. Wang, H.M.; Liu, Y.F. Microstructure and wear resistance of laser clad Ti₅Si₃/NiTi₂ intermetallic composite coating on titanium alloy. *Mater. Sci. Eng. A* **2002**, *338*, 126–132. [[CrossRef](#)]
9. Li, Y.H.; Yang, C.; Wang, F.; Zhao, H.D.; Qu, S.G.; Li, X.Q.; Zhang, W.W.; Li, Y.Y. Biomedical TiNbZrTaSi alloys designed by *d*-electron alloy design theory. *Mater. Des.* **2015**, *85*, 7–13. [[CrossRef](#)]
10. Pilone, D.; Brotzu, A.; Felli, F. Effect of surface modification on the stability of oxide scales formed on TiAl intermetallic alloys at high temperature. *Procedia Struct. Integr.* **2016**, *2*, 2291–2298. [[CrossRef](#)]
11. Ke, J.L.; Huang, C.H.; Chen, Y.H.; Tsai, W.Y.; Wei, T.Y.; Huang, J.C. In vitro biocompatibility response of Ti–Zr–Si thin film metallic glasses. *Appl. Surf. Sci.* **2014**, *322*, 41–46. [[CrossRef](#)]
12. Tkachenko, S.; Datskevich, O.; Kulak, L.; Jacobson, S.; Engqvist, H.; Persson, C. Wear and friction properties of experimental Ti–Si–Zr alloys for biomedical applications. *J. Mech. Behav. Biomed. Mater.* **2014**, *39*, 61–72. [[CrossRef](#)] [[PubMed](#)]
13. Rodrigues, G.; Nunes, C.A.; Suzuki, P.A.; Coelho, G.C. Thermal expansion of the Ti₅Si₃ and Ti₆Si₂B phases investigated by high-temperature X-ray diffraction. *Intermetallics* **2006**, *14*, 236–240. [[CrossRef](#)]
14. Yang, Y.; Chang, Y.A.; Tan, L. Thermodynamic modeling and experimental investigation of the Ti-rich corner of the Ti–Si–B system. *Intermetallics* **2005**, *13*, 1110–1115. [[CrossRef](#)]
15. Vojtěch, D.; Bártová, B.; Kubatík, T. High temperature oxidation of titanium–silicon alloys. *Mater. Sci. Eng. A* **2003**, *361*, 50–57. [[CrossRef](#)]
16. Hsu, H.-C.; Wu, S.-C.; Hsu, S.-K.; Li, Y.-C.; Ho, W.-F. Structure and mechanical properties of as-cast Ti–Si alloys. *Intermetallics* **2014**, *47*, 11–16. [[CrossRef](#)]
17. Ramos, E.C.T.; Silva, G.; Ramos, A.S.; Nunes, C.A.; Baptista, C.A.R.P. Microstructure and oxidation behavior of Ti–Si–B alloys. *Mater. Sci. Eng. A* **2003**, *363*, 297–306. [[CrossRef](#)]
18. Suryanarayana, C. Mechanical Alloying and Milling. *Prog. Mater. Sci.* **2001**, *46*, 1–184. [[CrossRef](#)]
19. Lee, Y.-S.; Lee, S.-M. Phase formation during mechanical alloying in the Ti–Si system. *Mater. Sci. Eng. A* **2007**, *449–451*, 1099–1101. [[CrossRef](#)]
20. Nunes, P.A.; Ramos, A.S.; Ramos, E.C.T. Effect of Molybdenum on the Formation of Ti₆Si₂B in Mechanically Alloyed Ti–Mo–Si–B Powders. *Mater. Sci. Forum* **2012**, *727*, 216–221. [[CrossRef](#)]
21. Taran-Zhovnir, Y.N. Laws of eutectic transformations in alloys. *Met. Sci. Heat Treat.* **1998**, *40*, 210–216. [[CrossRef](#)]
22. Zhan, Y.; Zhang, X.; Hu, J.; Guo, Q.; Du, Y. Evolution of the microstructure and hardness of the Ti–Si alloys during high temperature heat-treatment. *J. Alloys Compd.* **2009**, *479*, 246–251. [[CrossRef](#)]
23. Jiang, Z.; Dai, X.; Middleton, H. Effect of silicon on corrosion resistance of Ti–Si alloys. *Mater. Sci. Eng. B* **2011**, *176*, 79–86. [[CrossRef](#)]
24. Ramos, A.S.; Nunes, C.A.; Rodrigues, G.; Ramos, E.C.T. Effect of zirconium addition on the phase transformations in as-cast and heat-treated Ti–Zr–Si–B alloys. *J. Alloys Compd.* **2014**, *601*, 94–99. [[CrossRef](#)]
25. JCPDS: International Centre for Diffraction Data. *Powder Diffraction File (Inorganic Phases)*, 1st ed.; JCPDS: International Centre for Diffraction Data: Swarthmore, PA, USA, 1988; Volume 2.

26. Kraus, W.; Nolze, G. Powdercell—A program for the representation and manipulation of crystal structures and calculation of the resulting X-ray powder patterns. *J. Appl. Crystallogr.* **1996**, *29*, 301–303. [[CrossRef](#)]
27. Rodriguez-Carvajal, J. Recent Developments of the Program FULLPROF, in Commission on Powder Diffraction (IUCr). *Newsletter* **2001**, *26*, 12–19.
28. Yan, Z.H.; Oehring, M.; Bormann, R. Metastable phase formation in mechanically alloyed and ball milled Ti–Si. *J. Appl. Phys.* **1992**, *72*, 2478–2487. [[CrossRef](#)]
29. Oehring, M.; Bormann, R. Nanocrystalline alloys prepared by mechanical alloying and ball milling. *Mater. Sci. Eng. A* **1991**, *134*, 1330–1333. [[CrossRef](#)]
30. Ravi Chandran, K.S.; Panda, K.B.; Sahay, S.S. TiB_w-reinforced Ti composites: Processing, properties, application prospects, and research needs. *JOM* **2004**, *56*, 42–48. [[CrossRef](#)]
31. Li, C.; Zhan, Y.; Mo, Y.; She, J. In situ synthesized Ti₅Si₃/Ti–Mo lightweight structural composites. *Int. J. Refract. Met. Hard Mater.* **2013**, *41*, 432–436. [[CrossRef](#)]



© 2018 by the authors. Licensee MDPI, Basel, Switzerland. This article is an open access article distributed under the terms and conditions of the Creative Commons Attribution (CC BY) license (<http://creativecommons.org/licenses/by/4.0/>).